Turbulence and Energy Dissipation in the Developing Non-Aerated and the Fully-Developed Aerated Flows on a Stepped Spillway

G. Zhang
The University of Queensland, Australia, gangfu.zhang@uqconnect.edu.au

H. Chanson
The University of Queensland, Australia, h.chanson@uq.edu.au

6th International Symposium on Hydraulic Structures Portland, Oregon, USA, 27-30 June 2016
Hydraulic Structures and Water System Management
ISBN 978-1-884575-75-4 DOI: 10.15142/T3640628160853

Turbulence and Energy Dissipation in the Developing Non-Aerated and the Fully-Developed Aerated Flows on a Stepped Spillway

G. Zhang[1] and H. Chanson[1]
[1]Dept. of Civil Engineering
The University of Queensland
QLD 4072
Australia
E-mail: h.chanson@uq.edu.au

ABSTRACT

Stepped spillways are characterised by highly turbulent air-water flows and a large rate of energy dissipation compared to smooth chutes. Herein, detailed measurements were performed in both the developing non-aerated and fully-developed air-water flow regions on a large 1V:1H stepped spillway model. In the developing flow region, large total pressure fluctuations and turbulence intensities were recorded next to the pseudo-bottom. Downstream of the inception point, large total pressure fluctuations were recorded, which were mainly induced by density fluctuations. The water turbulence intensities in the air-water flow region did not differ significantly from those in the developing flow region. The steps generated significant form loss, amounting to about 50% of the upstream total energy regardless of discharge. Similar rates of energy dissipation and friction factors were found between the developing non-aerated and fully-developed air-water flow regions. The energy dissipation on stepped chutes was found to be sensitive to the chute slope and relatively little affected by the air-bubble diffusion.

Keywords: *Stepped spillways, energy dissipation, turbulence intensity, total pressure, macro-roughness, physical modelling.*

1. INTRODUCTION

Stepped spillways have been used as flood release structures for several centuries (Chanson 2001). The steps act as macro-roughness elements and greatly enhance the rate of energy dissipation. In practice, the design unit discharges on stepped chutes are typically large and correspond to the skimming flow regime (Matos 2000). In skimming flows, the water skims over the pseudo-bottom formed by the step edges and usually incorporates strong air-entrainment and turbulent mixing. The interplay between entrained air bubbles and coherent structures remains a challenging research topic (Chanson and Toombes 2002, Bung 2009).

It is the aim of this work to investigate the turbulence properties and energy dissipation performances of skimming flows and understand how they are affected by the air-bubble diffusion. New experiments were conducted in a large-size stepped spillway model (1V:1H) at the University of Queensland with a focus on skimming flows. The total pressure and two-phase flow properties at step edges were measured at the channel centreline via simultaneous sampling of a MEMS-based total pressure transducer and a phase-detection probe. The water-phase turbulence intensities are presented. The results suggest that the chute performances are little affected by air-bubble diffusion but may be sensitive to the geometry of the steps.

2. EXPERIMENTAL FACILITY AND INSTRUMENTATION

New experiments were performed in a large-size stepped spillway model at the University of Queensland. The experimental setup is sketched in Figure 1. The facility consisted of 12 flat steps made with smooth marine ply, each with dimensions 0.1 m length × 0.1 m height × 0.985 m width. The facility was previously used by Zhang and Chanson (2015). Total pressure measurements were taken in both the developing clear-water and fully-developed aerated flow regions at step edges along the chute centreline using a MEMS-based total pressure transducer with a

silicon diaphragm. The pressure transducer had an inner diameter of 1 mm and a precision of 0.5% (full scale). In the aerated flow region, the total pressure transducer was mounted beside a dual-tip phase-detection probe (0.25 mm inner diameter) that recorded the two-phase flow properties. The transverse separation between the two probes was 6.5 mm. The sampling rate and duration were 5 kHz per sensor and 60 s in the developing flow, and 5 kHz per sensor and 180 s in aerated flow region, following Wang et al. (2014). The vertical probe adjustment was controlled by a Mitutoyo™ digital scale with an accuracy of ±0.01 mm. The facility was operated at high Reynolds numbers ($Re = 4q/\nu$), up to 8.8×10^5. The experimental flow conditions are summarised in Table 1, where Q is the discharge, d_c is the critical flow depth, h is the vertical step height, and Re is the Reynolds number.

Table 1. Summary of experimental flow conditions

Study type	Q (m^3/s)	d_c/h	Location	Re
Developing flow Aerated flow	0.083 – 0.216	0.9, 1.1, 1.3, 1.5, 1.7	Step edges 3 – 9 Step edges 5 – 12	$3.9 \times 10^5 – 8.8 \times 10^5$

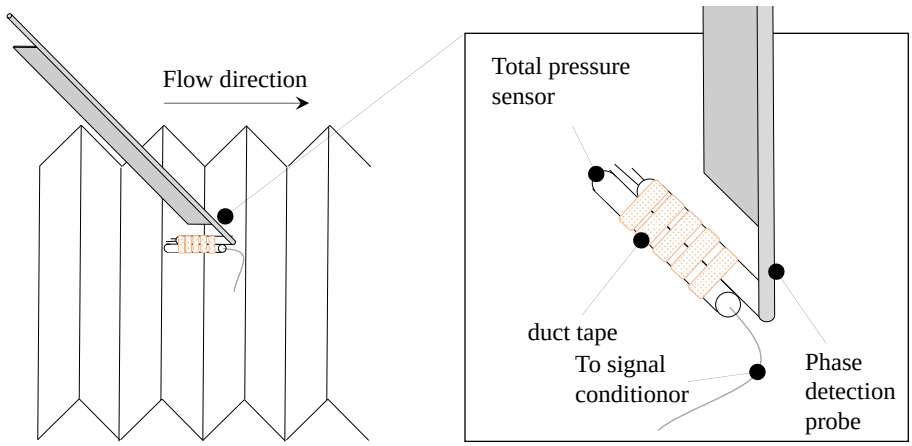

Figure 1. Sketch of experimental setup on the stepped chute at the University of Queensland

3. DEVELOPING FLOW REGION

Total pressure measurements were conducted with the MEMS total pressure transducer in the developing flow region at several step edges upstream of the inception point of free-surface aeration (Table 1). The probe was aligned in the direction of the main flow and recorded the instantaneous total pressure, expressed as

$$\tilde{P}_t = \frac{1}{2}\tilde{\rho}\tilde{U}^2 + \tilde{P}_s \tag{1}$$

where P_t is the total pressure, P_s is the static pressure, ρ is the fluid density, and U is the streamwise fluid velocity. Here and onwards, the overhead tilde (~), capital letters, and lower case letters are used to denote instantaneous, time-averaged, and fluctuating properties, respectively. At each measurement location, the time-averaged total head may be expressed as

$$H_t = \frac{P_t}{\rho_w g} + (1-C)z \tag{2}$$

where ρ_w is the water density, g is the gravity constant, C is the time-averaged void fraction, and z is the vertical elevation above the spillway toe. The dimensionless total head distributions are shown for two step edges in Figure 2, where y is the normal distance from the pseudo-bottom, δ is the boundary layer thickness (obtained from Zhang

and Chanson 2015), and $H_{t,crest}$ is the upstream total head measured with respect to the spillway toe. The data showed two distinct regions: a turbulent boundary layer in which significant viscous dissipation takes place ($y/\delta \leq 1$) and a potential flow region above governed by Euler equations ($y/\delta > 1$). The boundary between these two regions is shown with a horizontal dotted and dashed line in Figure 2.

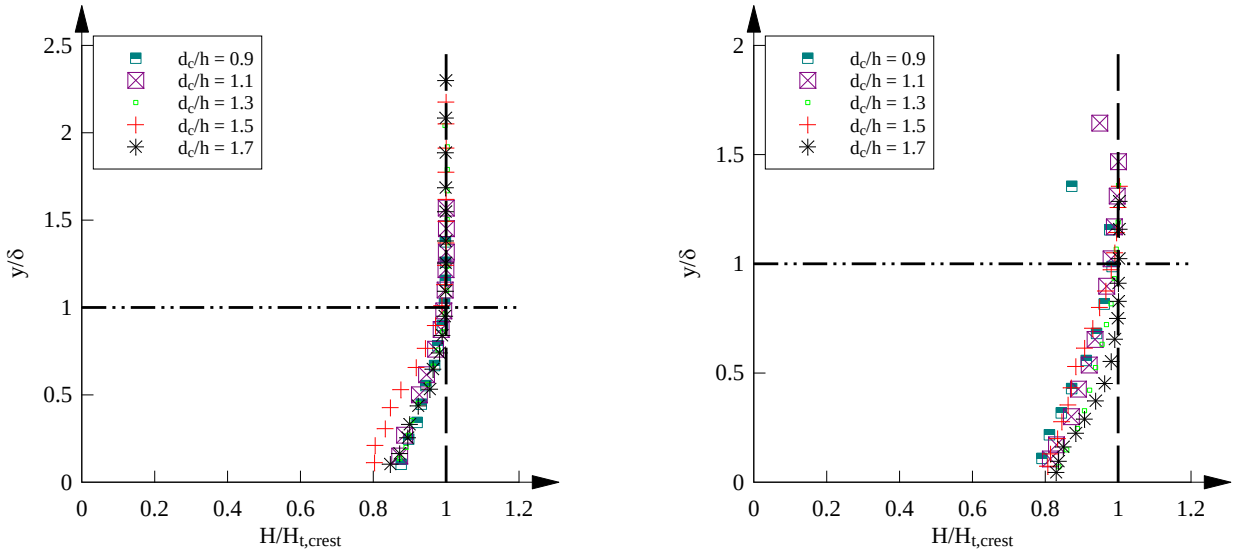

(A) Step edge 3 (B) Step edge 4

Figure 2. Total head distributions in the developing flow region – Flow conditions: d_c/h = 0.9, 1.1, 1.3, 1.5, 1.7; θ = 45°, h = 0.1 m

The boundary layer region ($y/\delta \leq 1$) is characterised by strong boundary-induced turbulent fluctuations and significant viscous dissipation. The lowest order descriptor of the turbulence properties is the turbulence intensity, defined in terms of the local water velocity U_w:

$$Tu = \frac{< u_w^2 >^{0.5}}{U_w} \quad (3)$$

where <> is the averaging operator. When the static pressure fluctuation (p_s) is small and the turbulent water velocity data (u_w) follow a normal distribution, the turbulence intensity may be derived from Equation (1) by subtracting its mean from the original Equation (1), squaring both sides and taking the mean, dividing by $\rho_w U_w^2$ and square-rooting the result. The development yields a relationship between the turbulence intensity and the total pressure fluctuations:

$$Tu = \frac{< p_t^2 >^{0.5}}{\rho_w U_w^2} \quad (4)$$

Arndt and Ippen (1970) derived the same equation and suggested a maximum error of about 5% for a turbulence intensity of 10%. Figure 3 presents typical turbulence intensity distributions in skimming flows at step edges 3 and 4. The streamwise velocity (U_w) and boundary layer thickness (δ) data were measured by Zhang and Chanson (2015) for the same flow conditions in the same facility. For all present data, the largest turbulence intensities were observed next to the pseudo-bottom formed by the step edges. Maximum turbulence intensity values Tu_{max} ranged between 0.3 and 0.45 and decreased with increasing distance from the pseudo-bottom. Next to the boundary layer outer edge ($y/\delta \approx 1$), Tu was about 0.05. Interestingly, non-trivial values of Tu were observed up to y/δ = 1.2 – 1.4, which might arise from irrotational velocity fluctuations in the external flow induced by boundary layer turbulence (Zhang and Chanson 2015). The present data were close to those obtained using PIV (Amador et al. 2006) on a

51.3° steppe chute and those in flows over transverse rib-roughness (Okamoto et al. 1993, Cui et al. 2003). This demonstrates that the probe had an adequate frequency response for turbulence measurements.

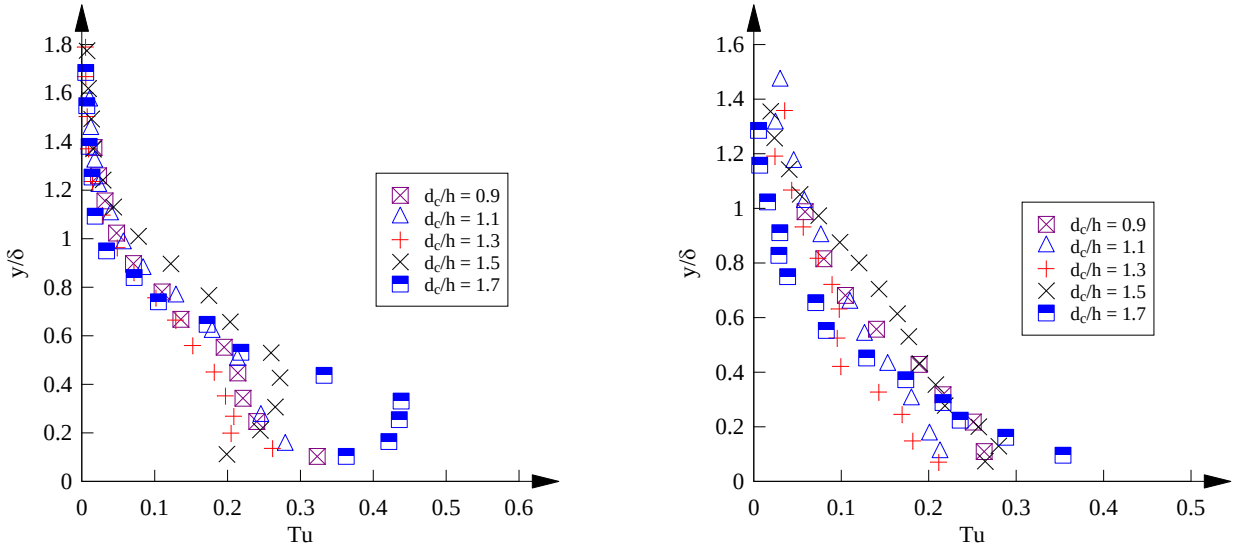

(A) Step edge 3 (B) Step edge 4

Figure 3 – Turbulence intensity distributions in the developing flow region

4. FULLY-DEVELOPED AIR-WATER FLOW REGION

Downstream of the inception point of free-surface aeration, the stepped spillway flow was characterised by strong air-entrainment and turbulent mixing. Typical distributions of time-averaged void fraction (C) and bubble count rate (F) are shown in Figure 4, where F_{max} is the maximum bubble count rate at one cross-section. The void fraction distribution followed an S-shaped distribution typical of skimming flows (Chanson and Toombes 2002, Gonzalez and Chanson 2008, Bung 2009, Felder and Chanson 2011). The data may be described by a solution of the advection-diffusion equation (Chanson and Toombes 2002):

$$C = 1 - \tanh^2\left(K - \frac{y/Y_{90}}{2D_0} + \frac{\left(y/Y_{90} - 1/3\right)^2}{3D_0}\right) \quad (5)$$

where Y_{90} is the depth where C = 0.9, K is an integration constant and D_0 is a function of the depth-averaged void fraction. Equation (5) is compared to experimental data in Figure 4. A good agreement is observed, despite of some underestimation for y/d_c < 0.3. This might be a result of bubbles trapped in vortices shed from the upstream step edge.

Defined as the number of air-to-water interfaces detected by the probe sensor per second, the bubble count rate is proportional to the specific interfacial area (Chanson 2002). In Figure 4, typical data are presented, showing a characteristic shape with a maximum value at about y/d_c = 0.4 (C = 0.4 – 0.5). The observation is consistent with past studies on stepped chute flows (e.g. Chanson and Toombes 2002). It was demonstrated (Toombes and Chanson 2008) that the bubble count rate is positively correlated with the void fraction variance (deduced from a binary signal) equalling $C(1\text{-}C)$ (Chanson and Carosi 2007), which is maximum at C = 0.5.

The aerated flow region exhibited strong total-pressure fluctuations although its characteristic magnitude (i.e. $<p_t^2>^{1/2}$) may not be a good descriptor of the water-phase turbulence because these fluctuations are mostly induced by the density fluctuations (i.e. change in density between air and water as bubbles are detected by the MEMS sensor) when a large number of air-water interfaces is present. In Figure 5, the characteristic total pressure

fluctuation is plotted against the bubble count rate for one discharge (d_c/h = 0.9), where $<p_t^2>_{max}^{1/2}$ is the maximum characteristic total pressure fluctuation at each cross-section. The data indicated a strong positive correlation between total pressure fluctuations and bubble count rate. Some hysteresis around F/F_{max} = 1 was observed, likely caused by wall effects that were mainly concentrated in the lower air-water flow column. Note that $<p_t^2>^{1/2}/<p_t^2>_{max}^{1/2} \approx 0.2 - 0.3$ next to the free-surface for $F/F_{max} \approx 0$ (refer to Figure 4), which was likely because of system noise and capillary effects.

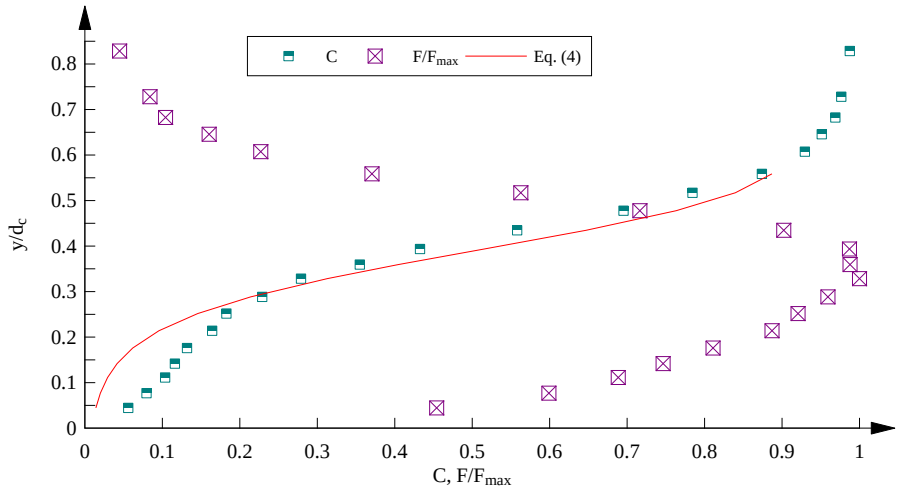

Figure 4. Typical void fraction and bubble count rate distributions in skimming flows – Flow conditions: d_c/h = 1.1, step edge 12; θ = 45°, h =0.1 m

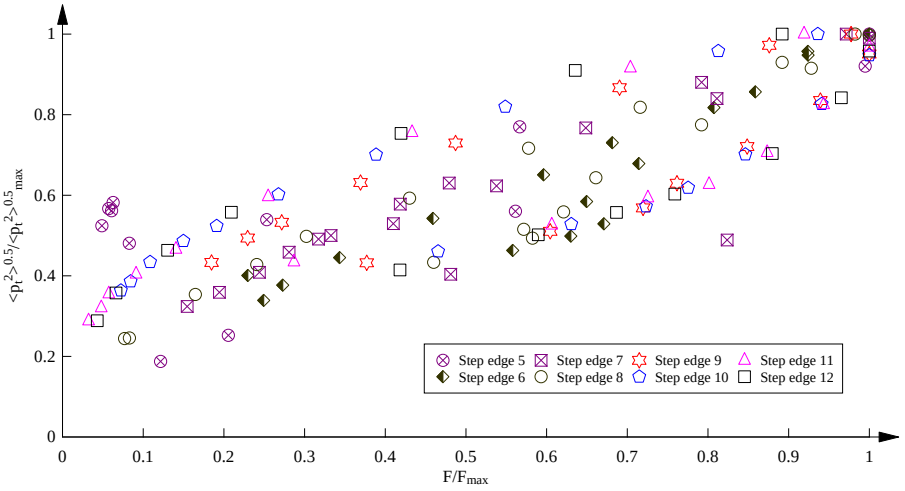

Figure 5. Relationship between dimensionless bubble count rate and total pressure fluctuations – Flow conditions: d_c/h = 0.9, θ = 45°, h = 0.1 m

For an aerated flow, the water-phase turbulence intensity Tu (Equation (3)) may be derived from Equation (1) using a similar technique as discussed in Section 3. The result yields a relationship between the water-phase turbulence intensity, total pressure standard deviation, time-averaged velocity, and time-averaged void fraction (Zhang and Chanson 2016b):

$$Tu = \sqrt{\frac{< p_t^2 >}{\rho_w^2 U_w^4} - \frac{C(1-C)}{4}} \Big/ \left(\left(1+\frac{1}{2}C\right)(1-C)\right) \quad (6)$$

The derivation of Equation (6) assumes (a) no-slip between phases: i.e., $U = U_w = U_a$; (b) the density of air is zero; (c) the static pressure fluctuation and capillary effects are negligible; and (d) both the transitions between air and water phases and the probe sensor response are instantaneous. Note that Equation (6) becomes inaccurate for $Tu >$ 0.4 – 0.5 because higher order terms were neglected in its derivation. Figure 6 shows typical water-phase turbulence intensity distributions at each step edge downstream of the inception point for four skimming flow conditions, where the void fraction and velocity data were obtained from phase-detection probe signals (Section 2). All data showed turbulence intensity of the water phase between 0.1 and 0.5, irrespective of the flow rate. Local maxima were found next to the pseudo-bottom, ranging between 0.2 – 0.4. The turbulence intensity decreased with increasing distance from the pseudo-bottom with minimum values of about 0.1 – 0.15 next to $y/d_c = 0.3$ ($C = 0.4 – 0.5$). For $y/d_c > 0.3$, the data generally increased with increasing distance from the pseudo-bottom despite showing large scatter. Note that *Tu* presented minimum values next to locations of maximum bubble count rates ($y/d_c \approx 0.3$). This suggested that a large number of bubbles might introduce an effective spring constant that reduced the rate-of-strain of the water particles. Overall, the aerated flow region exhibited turbulence intensities of the same order of magnitude of, albeit with a much more uniform distribution than, those in the developing clear-water flow region.

5. ENERGY DISSIPATION IN SKIMMING FLOWS

On a stepped chute, a significant fraction of the kinetic energy is dissipated by turbulence generated by the stepped invert. For the clear-water developing and aerated fully-developed flow regions, the depth-averaged total head is defined as

$$H_d = \frac{1}{d}\int_0^d H_t dy \quad \text{for the developing flow region} \quad (7)$$

$$H_d = \frac{1}{d_e}\int_0^{Y_{90}} H_t dy \quad \text{for the aerated flow region} \quad (8)$$

where $d_e = \int_0^{Y_{90}} (1-C) dy$ is the equivalent clear water depth in the aerated flow region and Y_{90} is the normal distance to the pseudo-bottom from where $C = 0.9$. Figure 7A shows the distributions of H_d along the chute centreline for two skimming discharges, normalised by $H_{t,crest}$. For all discharges, the total head decreased monotonically along the stepped chute. The overall energy dissipation was about 50% of the upstream total head, a result comparable to previous investigations (e.g. Felder and Chanson 2009, 2011, 2014). A closer examination showed some see-saw pattern with a wave length of about 1-2 cavity lengths, which was most evident for the largest discharge ($d_c/h = 1.7$). Such a see-saw pattern in the longitudinal distributions of characteristic air-water flow parameters (e.g. Y_{90}/d_c, V_{90}/V_c) was observed previously (e.g. Matos 2000, Felder and Chanson 2009), supporting the argument by several authors (Chanson et al. 2002, Chanson 2006, Felder and Chanson 2009) that uniform equilibrium conditions might not exist on stepped chutes.

Figure 7B presents the residual head H_{res} (i.e. H_d at the last step edge) normalised by the critical depth d_c. The present data were compared to those in 26.6° chutes with flat steps (Felder and Chanson 2011, 2014) and the reanalysis of the data of Zhang and Chanson (2014) in a 26.6° gabion stepped chute (solid symbols: flat steps; hollow symbols: gabion steps). For all configurations, the residual head generally decreased with increasing discharge. For a given discharge, the residual head was the largest in the 26.6° gabion chute, followed by the present setup. On the gabion chute, form drag was significantly reduced because of ventilation of the step cavities and the interactions between seepage and cavity flows (Zhang and Chanson 2016a). The larger residual head on the present

facility (θ = 45º) compared to the 26.6° chutes with flat steps suggested that the energy dissipation performance was a function of the cavity geometry. A larger cavity aspect ratio (step length/height) might improve the efficiency of energy dissipation by reducing the shedding effects of each roughness element (i.e. step) on the subsequent one.

The significant rate of energy dissipation in stepped chutes was attributed mostly to form loss induced by the steps (Rajaratnam 1990, Chanson 2001, Chanson et al. 2002). The flow is commonly assumed to be quasi-smooth, and the flow resistance is typically expressed using the Darcy-Weisbach friction factor (Rajaratnam 1990, Chanson 2001):

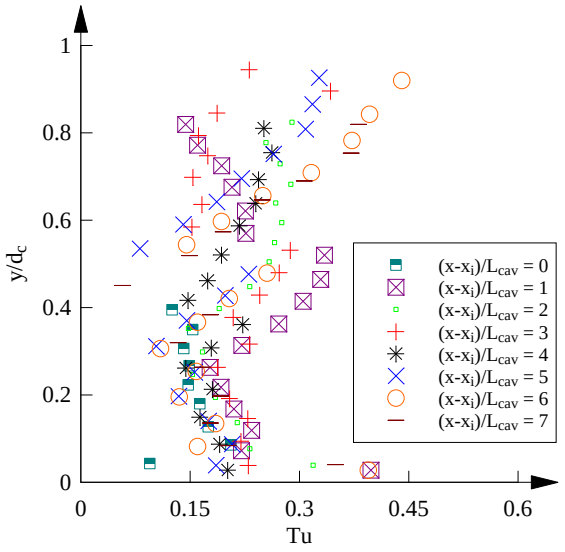

(A) d_c/h = 0.9

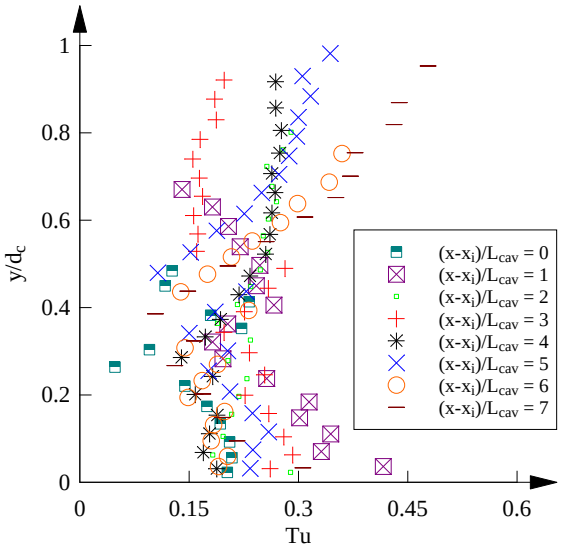

(B) d_c/h = 1.1

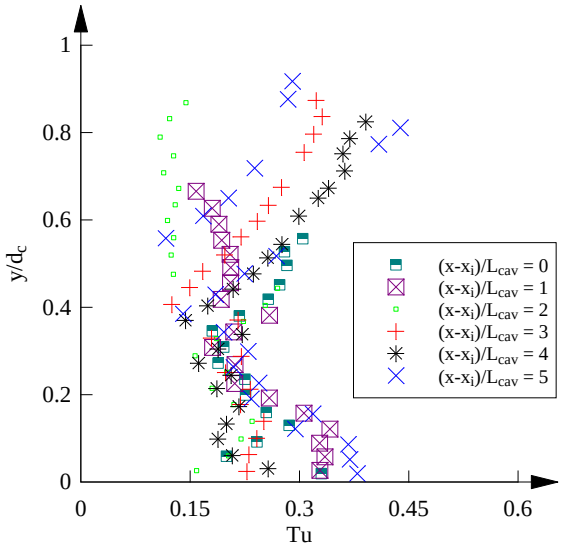

(C) d_c/h = 1.3

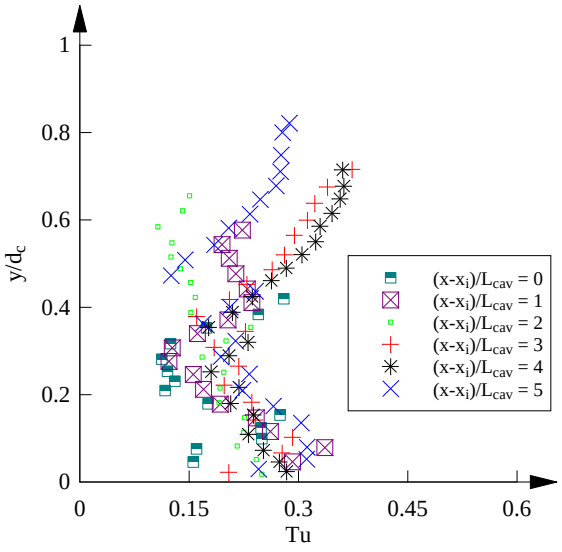

(D) d_c/h = 1.5

Figure 6. Water phase turbulence intensity at step edges – Flow conditions: d_c/h = 0.9, 1.1, 1.3, 1.5; θ = 45°, h = 0.1 m

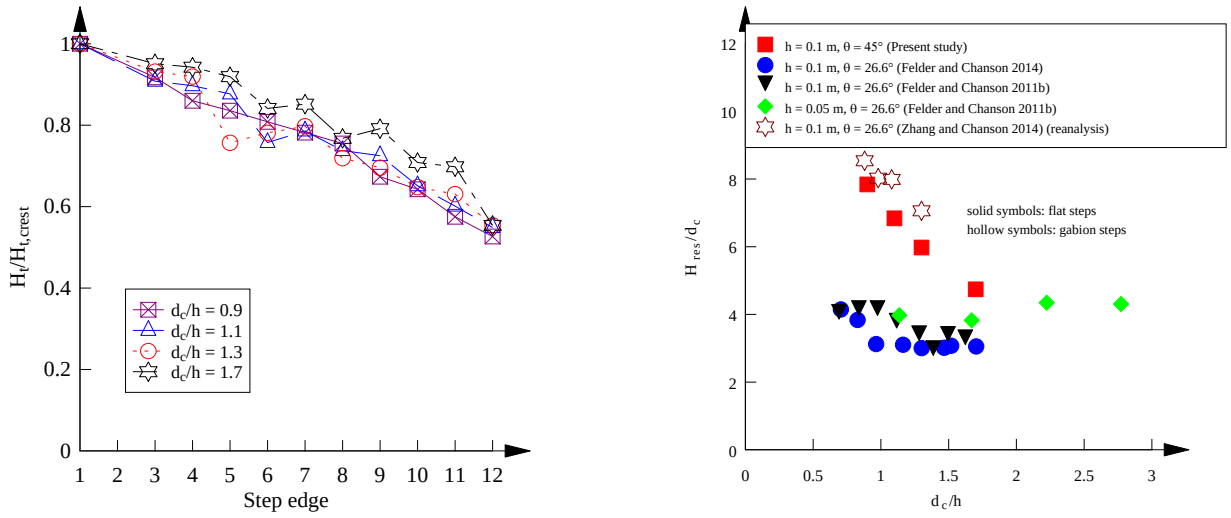

(A) Depth averaged total head along stepped chute (B) Residual head above the last step edge

Figure 7. Energy dissipation along stepped chutes

$$f_e = 8S_f \left(\frac{d}{d_c}\right)^3 \quad \text{for clear water flow (9)}$$

$$f_e = 8S_f \left(\frac{d_e}{d_c}\right)^3 \quad \text{for air-water flow (10)}$$

where S_f is the friction slope: i.e., the slope of the total head line. Note that Equations (9) and (10) are only valid for fully developed skimming flows in a wide rectangular channel and may be inappropriate to quantify form losses (Chanson 2001). Present data are plotted in Figure 8, where D_H is the hydraulic diameter. For each discharge, the friction factor was calculated for (a) the clear-water developing flow region upstream of the visually-defined inception point; (b) the air-water flow region downstream of the inception point; and (c) the entire stepped chute (step edge 1 – 12). In the clear-water developing flow, the friction factor was on average $f_e \approx 0.19$, close to the findings of Zhang and Chanson (2015) obtained with a Prandtl-Pitot tube in the same chute. In the aerated flow region, the friction factors are slightly higher, with an average of $f_e \approx 0.27$. The present data are compared to those in stepped chutes with a 26.6° slope (Felder and Chanson 2011, Felder and Chanson 2014). For a given discharge, the present data are generally smaller than those in the 26.6° chutes with the same step height (h = 0.10 m). The data obtained with h = 0.05 m showed a different trend that could be linked to scale effects (Felder and Chanson 2011, 2014, 2015). A negative correlation between friction factors and dimensionless roughness height is observed for all data, which is characteristic of form losses.

6. CONCLUSION

New experiments were performed in a large-size stepped spillway model with a 45° slope (1V:1H) and uniform step heights of 0.1 m, with a focus on skimming flows. The total pressure distribution and two-phase flow properties were recorded via simultaneous sampling of a MEMS-based total pressure sensor and a dual-tip phase-detection probe. The water-phase turbulence intensity and energy dissipation performances were reported for both the developing clear-water and fully-developed air-water flow regions.

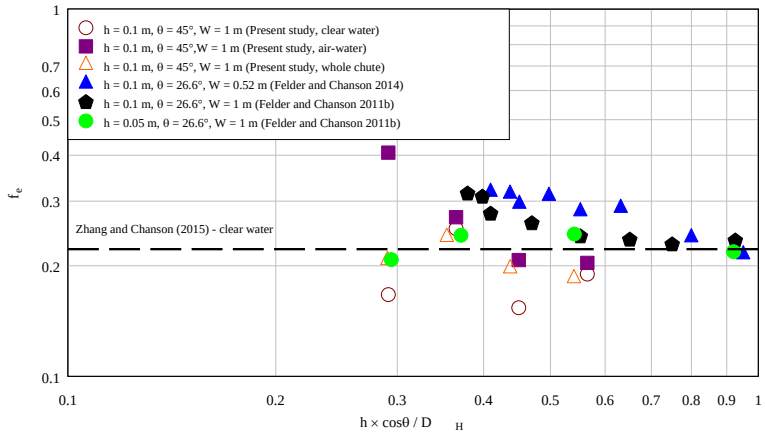

Figure 8. Darcy-Weisbach friction factors in skimming flows above stepped chutes – Flow conditions: d_c/h = 0.9, 1.1, 1.3, 1.5, θ = 45°, h = 0.1 m (Present study) - Solid symbols indicate air-water data.

The developing flow region consisted of a boundary layer and an irrotational flow region above. In the boundary layer, large total pressure fluctuations and turbulence intensities were recorded, while the potential flow region was governed by the Euler equations. The aerated flow region was characterised by strong air-entrainment and turbulent mixing. Large total pressure fluctuations were recorded, mainly induced by density fluctuations. The water phase turbulence intensities were similar to those in the developing flow region. The overall energy dissipation was about 50% of the upstream total head regardless of discharge. The rate of energy dissipation and friction factors were found to be similar in both the developing clear-water and fully-developed air-water flow regions. The present findings showed that energy dissipation performance of stepped chutes might not be much affected by air-bubble diffusion and might be sensitive to the step cavity geometry.

7. ACKNOWLEDGEMENTS

The authors owe their thanks to Dr. Hang Wang (The University of Queensland) for the initial setup of the total pressure transducer. The technical assistance of Jason Van Der Gevel and Stewart Matthews (The University of Queensland) is acknowledged. The financial support through the Australian Research Council (Grant DP120100481) is acknowledged.

8. REFERENCES

Amador, A., Sánchez-Juny, M. and Dolz, J. (2006). "Characterization of the nonaerated flow region in a stepped spillway by PIV." *Journal of Fluids Engineering*, Transactions of the ASME, Vol. 128, No. 6, pp. 1266-1273 (DOI: 10.1115/1.2354529).

Arndt, R.E.A. and Ippen, A.T. (1970). "Turbulence measurements in liquids using an improved total pressure probe." *Journal of Hydraulic Research*, Vol. 8, No. 2, pp. 131-158 (DOI: 10.1080/00221687009500300).

Bung, D.B. (2009). "Zur selbstbelüfteten Gerinnenströmung auf Kaskaden mit gemässigter Neigung." ("Self-aerated skimming flows on embankment stepped spillways.") *Ph.D. thesis*, University of Wuppertal, LuFG Wasserwirtschaft and Wasserbau, Germany, 292 pages (in German).

Chanson, H. (2001). "The hydraulics of stepped chutes and spillways." Balkema, Lisse, The Netherlands, 418 pages.

Chanson, H. (2002). "Air-water flow measurements with intrusive phase-detection probes. Can we improve their interpretation?" *Journal of Hydraulic Engineering*, ASCE, Vol. 128, No. 3, pp. 252-255 (DOI: 10.1061/(ASCE)0733-9429(2002)128:3(252)).

Chanson, H. (2006). "Hydraulics of skimming flows on stepped chutes: the effects of inflow conditions?" *Journal of Hydraulic Research*, IAHR, Vol. 44, No. 1, pp. 51-60 (DOI: 10.1080/00221686.2006.9521660).

Chanson, H., and Carosi, G. (2007). "Advanced post-processing and correlation analyses in high-velocity air-water flows." *Environmental Fluid Mechanics*, Vol. 7, No. 6, pp. 495-508 (DOI: 10.1007/s10652-007-9038-3).

Chanson, H., and Toombes, L. (2002). "Air-Water flows down stepped chutes. Turbulence and flow structure observations." *International Journal of Multiphase Flow*, Vol. 28, No. 11, pp. 1737-1761 (DOI: 10.1016/s0301-9322(02)00089-7).

Chanson, H., Yasuda, Y., and Ohtsu, I. (2002). "Flow resistance in skimming flows and its modelling." *Canadian Journal of Civil Engineering*, Vol. 29, No. 6, pp. 809-819 (DOI: 10.1139/l02-083).

Cui, J., Patel, V.C. and Lin, C. (2003). "Large-eddy simulation of turbulent flow in a channel with rib roughness." *International Journal of Heat and Fluid Flow*, Vol. 24, No. 3, pp. 372-388 (DOI: 10.1016/s0142-727x(03)00002-x).

Felder, S., and Chanson, H. (2009). "Energy dissipation, flow resistance and gas-liquid interfacial area in skimming flows on moderate-slope stepped spillways." *Environmental Fluid Mechanics*, Vol. 9, No. 4, pp. 427-441 (DOI: 10.1007/s10652-009-9130-y).

Felder, S., and Chanson, H. (2011). "Air-water flow properties in step cavity down a stepped chute." *International Journal of Multiphase Flow*, Vol. 37, No. 7, pp. 732–745 (DOI: 10.1016/j.ijmultiphaseflow.2011.02.009).

Felder, S., and Chanson, H. (2014). "Effects of step pool porosity upon flow aeration and energy dissipation on pooled stepped spillways." *Journal of Hydraulic Engineering*, ASCE, Vol. 140, No. 4, Paper 04014002, 11 pages (DOI: 10.1061/(ASCE)HY.1943-7900.0000858).

Felder, S., and Chanson, H. (2015). "Scale effects in high-velocity air-water flows on a stepped spillway." *Proc. 36th IAHR World Congress*, The Hague, The Netherlands, 27 June-3 July, Paper 81132, 9 pages.

Gonzalez, C.A., and Chanson, H. (2008). "Turbulence manipulation in embankment stepped chute flows: an experimental study." *European Journal of Mechanics B/Fluids*, Vol. 27, No. 4, pp. 388-408 (DOI: 10.1016/j.euromechflu.2007.09.003).

Matos, J. (2000). "Hydraulic design of stepped spillways over RCC dams." *Proc. The International Workshop on Hydraulics of Stepped Spillways*, Zürich, March 22-24, 2000, pp. 187-194.

Okamoto, S., Seo, S., Nakaso, K. and Kawai, I. (1993). "Turbulent shear flow and heat transfer over the repeated two-dimensional square ribs on ground plane." *Journal of Fluids Engineering*, Transactions of the ASME, Vol. 115, No. 4, pp. 631-637 (DOI: 10.1115/1.2910191).

Rajaratnam, N. (1990). "Skimming flow in stepped spillways." *Journal of Hydraulic Engineering*, ASCE, Vol. 116, No. 4, pp. 587-591 (DOI: 10.1061/(asce)0733-9429(1990)116:4(587)).

Toombes, L., and Chanson, H. (2008). "Interfacial aeration and bubble count rate distributions in a supercritical flow past a backward-facing step." *International Journal of Multiphase Flow*, Vol. 34, No. 5, pp. 427-436 (DOI: 10.1016/j.ijmultiphaseflow.2005.01.005).

Wang, H., Murzyn, F., and Chanson, H. (2014). "Total pressure fluctuations and two-phase flow turbulence in hydraulic jumps." *Experiments in Fluids*, Vol. 55, No. 11, Paper 1847, 16 pages (DOI: 10.1007/s00348-014-1847-9).

Zhang, G., and Chanson, H. (2014). "Step cavity and gabion aeration on a gabion stepped spillway." *Proc. 5th IAHR International Symposium on Hydraulic Structures*, 25-27 June 2014, Brisbane, Australia, H. Chanson and L. Toombes Editors, 8 pages (DOI: 10.14264/uql.2014.37).

Zhang, G., and Chanson, H. (2015). "Hydraulics of the developing flow region of stepped cascades: an experimental investigation." *Hydraulic Model Report No. CH97/15*, School of Civil Engineering, The University of Queensland, Brisbane, Australia, 76 pages.

Zhang, G., and Chanson, H. (2016a). "Gabion stepped spillway: interactions between free-surface, cavity and seepage flows." *Journal of Hydraulic Engineering*, ASCE (DOI: 10.1061/(ASCE) 11 HY.1943-7900.0001120).

Zhang, G., and Chanson, H. (2016b). "Interaction between free-surface aeration and total pressure on a stepped chute." *Experimental Thermal and Fluid Science*, Vol. 74, pp. 368-381 (DOI: 10.1016/j.expthermflusci.2015.12.011).